Performance Study of Strained III-V Materials for Ultra-Thin Body Transistor Applications

Martin Rau[*], Troels Markussen[†], Enrico Caruso[‡], David Esseni[‡], Elena Gnani[§], Antonio Gnudi[§], Petr A. Khomyakov[*], Mathieu Luisier[*], Patrik Osgnach[‡], Pierpaolo Palestri[‡], Susanna Reggiani[§], Andreas Schenk[*], Luca Selmi[‡] and Kurt Stokbro[†]

[*]Integrated Systems Laboratory, ETH Zürich, Zürich, Switzerland
[†]QuantumWise A/S, Copenhagen, Denmark
[‡]DIEGM, Universitá degli studi di Udine, Udine, Italy
[§]DEIS-ARCES, Universitá degli studi di Bologna, Bologna, Italy

***Abstract*—A comprehensive description of band gap and effective masses of III-V semiconductor bulk and ultra-thin body (UTB) structures under realistic biaxial and uniaxial strain is given using numerical simulations from four different electronic structure codes. The consistency between the different tools is discussed in depth. The nearest neighbor $sp^3d^5s^*$ empirical tight-binding model is found to reproduce most trends obtained by *ab initio* Density Functional Theory calculations at much lower computational cost. This model is then used to investigate the impact of strain on the ON-state performance of realistic $In_{0.53}Ga_{0.47}As$ UTB MOSFETs coupled with an efficient method based on the well-known top-of-the-barrier model. While the relative variation of effective masses between unstrained and strained cases seems promising at first, the calculations predict no more than 2% performance improvement on drive currents from any of the studied strain configurations.**

Keywords—III-V semiconductors; strain engineering; Density Functional Theory; Tight-binding; k·p; Ultra-Thin Body MOSFET; band structure; top-of-the-barrier model

I. INTRODUCTION

Strain engineering is an established technology booster for high-performance silicon MOSFETs [1]. Compressive (p-type) or tensile (n-type) stress greatly enhance the injection velocity of charge carriers leading to a significant increase of the devices' ON-performance. For III-V semiconductors, however, very little data on strain-induced performance improvement is available. Progress in that area could spark further interest in III-V semiconductors as the n-type materials of choice along with p-type germanium for next generation CMOS applications. As a reminder, III-V materials currently rank among the most promising n-type silicon-replacement candidates due to their much higher electron mobilities and injection velocities [2].

This paper is an attempt to answer the question whether realistic strain configurations may improve the performance of III-V-based MOSFETs by means of an extensive computational study involving four different band structure models - **k·p**, Empirical Tight-Binding (TB), and two types of Density Functional Theory (DFT).

First, a thorough description of bulk band structure parameters (band gap E_G and effective masses m^* along various crystal orientations) of GaAs and InAs under realistic biaxial and uniaxial strain is given.

The investigation on bulk is then extended to more time-consuming simulations of $In_{0.53}Ga_{0.47}As$ ultra-thin body (UTB) channels of thicknesses ranging from 10 nm down to 3 nm. At each step of the study, the high-level models (**k·p** and TB) are compared to *ab initio* calculations (DFT) to identify the best suited tool for complete device simulations. The most promising high-level tool is then used to assess the effect of strain engineering on the ON-state performance of realistic UTB devices by coupling results from band structure calculations to the widely used top-of-the-barrier (ToB) model [3]. This method avoids time-consuming self-consistent simulations while preserving the essential physics involved in strain-induced ON-performance variations.

II. MODELS

Simulations within the DFT formalism have been performed with two distinct models. The first one, implemented in ATK-2015 [4], uses the meta-generalized gradient approximation exchange correlation functional of Tran and Blaha (TB09) [5]. This functional contains a so-called *c-parameter* used to adjust the band gap to best fit experimental data on bulk materials. This model will be referred to as 'DFT(i)' from now on.

The second DFT model, available in the VASP code [6], makes use of the hybrid functional approach (HSE06) [7] combined with a plane-wave pseudopotential approach [8]. Additional technical details about this method can be found in [9]. This model is labeled 'DFT(ii)' from now on.

Simulations in the nearest neighbor empirical TB formalism with spin-orbit coupling are performed using OMEN [10]. To model the strained and unstrained bulk and confined structures, the $sp^3d^5s^*$ TB and strain parameters of [11] [12] have been utilized as they provide a good agreement with available experimental data. We further apply the virtual crystal approximation [12] to deal with the ternary compound $In_{0.53}Ga_{0.47}As$.

The **k·p** calculations are performed using an 8-band model of strained zinc-blende crystals [13] [14].

III. STRAIN CONFIGURATIONS

In this study, systems under compressive/tensile biaxial and uniaxial strain are considered without any ion relaxation, *i.e.* the atoms are displaced with respect to the applied strain

tensor, but no additional geometry optimization is performed. With DFT and TB, the atom coordinates of the strained structure are used to create a new Hamiltonian matrix used for band structure calculations, while with the **k·p** method, a strain-tensor-dependent matrix is directly added to the unstrained Hamiltonian matrix [13]. The presence of interface states whose impact on the free electron charge in the channel may be modulated by strain [15] has not been considered.

For DFT and TB, the values of the elastic constants used to calculate the deformation along the directions where no stress is applied are taken from [16] for both GaAs and InAs. For **k·p**, the values from [17] ensure full consistency between models. Both sets of values are very similar. For $In_{0.53}Ga_{0.47}As$, a linear interpolation between the values of GaAs and InAs is done. In all plots, ε is defined as the strain along the direction of external stress (two for biaxial and one for uniaxial). It varies between -2% (compressive) and 2% (tensile). This choice covers the most relevant strain interval from the technological point of view.

A. Biaxial Strain

In the biaxial strain case, the *x*-, *y*-, and *z*-axes of the coordinate system are aligned along the [100], [001] and [010] crystal orientations respectively, while biaxial stress is applied along [100] and [010]. In this case, the strain values along the x and z axes are equal, *i.e.* $\varepsilon=\varepsilon_{xx}=\varepsilon_{zz}$. The strain along the y axis, ε_{yy}, is calculated following [18]. For UTBs, the confinement direction is chosen to be the [001] axis.

B. Uniaxial Strain

The technologically relevant case here is to apply uniaxial stress along the [110] axis. The *x*-, *y*-, and *z*-axes are then aligned with the [110], [001], and [-110] crystal orientations respectively. In this case, $\varepsilon=\varepsilon_{xx}$ and the strain components ε_{yy} and ε_{zz} are again calculated following [18]. For UTBs, the confinement direction is chosen to be the [001] axis.

IV. Results

A. Band gap and effective masses in strained bulk GaAs/InAs

1) Biaxial strain

Figs. 1 and 2 show the variation of E_G and m^* along [100] and [001] for bulk GaAs and InAs, respectively, under compressive and tensile biaxial strain as defined in Section III.

Tensile biaxial strain decreases E_G, while compressive strain increases it. For both GaAs and InAs, compressive strain has a smaller effect on E_G compared to tensile strain.

Tensile biaxial strain decreases the effective masses along [100] and [001], while compressive strain increases them. Compared to E_G, there is a nearly monotonous decrease of m^* from compressive to tensile strain in all models, although the predicted slopes differ. While TB agrees better than **k·p** with DFT along [100], **k·p** agrees better than TB with DFT along [001]. The relatively large differences in the absolute values of the effective masses between DFT(i) and TB/**k·p** are due to the *c*-parameter introduced in Section II. It leads to an overestimation of the effective masses when it is adjusted to best reproduce the measured E_G. Since trends are well captured by all models, the validity of the results is reinforced.

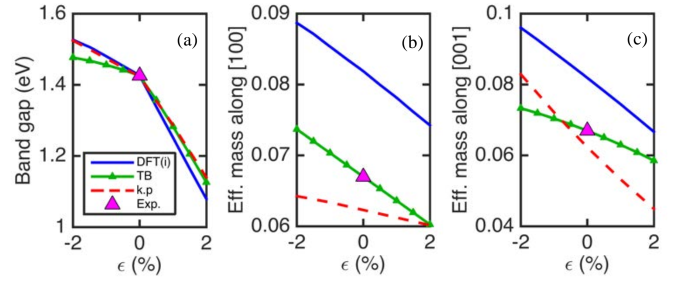

Fig. 1 Biaxial strain in bulk GaAs. (a) Band gap at Γ. (b) Electron effective mass (units of m_0) along the [100] crystal axis. (c) Same as (b), but along the [001] axis.

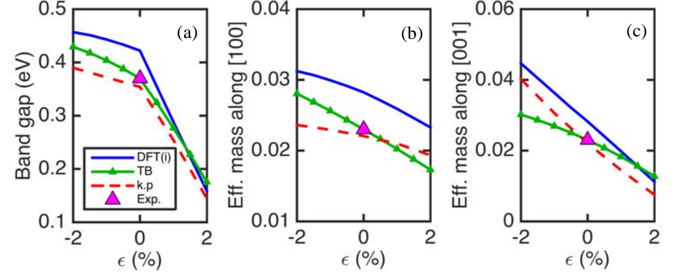

Fig. 2 Same as Fig. 1, but for InAs.

2) Uniaxial strain

Figs. 3 and 4 show the variation of E_G and m^* along the [110], [001] and [-110] directions for bulk GaAs and InAs, respectively, under compressive and tensile uniaxial strain as defined in Section III. The agreement between the models is not as good as in the biaxial strain case, which is why results obtained with DFT(ii) have been added to provide an additional basis for comparison.

For both materials, the general behavior of E_G under uniaxial strain is similar to the one obtained in the biaxial case. Putting aside the previously discussed offsets in absolute value, the two DFT models predict the same trend. Thus, their status as a reference for comparison and calibration of high-level models is confirmed. The less-pronounced effect on E_G of compressive versus tensile strain is observed again.

A more fundamental discrepancy is found between **k·p** and the other models about the variation with strain of the effective masses along [110] in GaAs and InAs. While TB and the two DFT models predict a decrease in effective mass when varying strain from compressive to tensile, **k.p** predicts an increase. A similar disagreement is found for the effective mass along [-110] in GaAs, although to a somewhat lesser extent. A different software implementation of the **k·p** model led to the same results. It can thus be safely assumed that this discrepancy is intrinsic to the **k·p** formalism. A thorough re-calibration of the **k.p** parameters using TB band structure data led to an effective mass which is rather flat with respect to strain along both [110] and [-110] (Fig. 3 (b) and (d)), only partially reconciling the disagreement. Further investigations will be needed to get additional insights.

As the predicted slopes for all effective masses agree very well between TB and the two DFT models, especially with DFT(ii) which is thought to be the most accurate, TB is the method of choice for future device performance analysis.

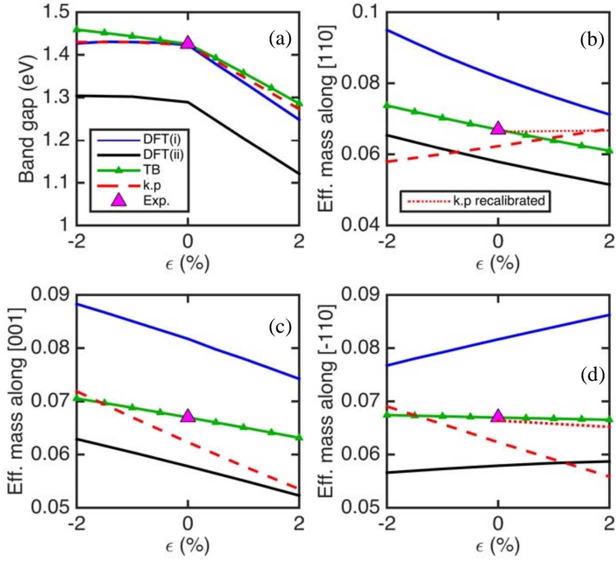

Fig. 3 Bulk GaAs under uniaxial strain. (a) Band gap at Γ. (b) Electron effective mass (units of m_0) along the [110] crystal axis. (c) Same as (b), but along [001]. (d) Same as (b), but along [-110].

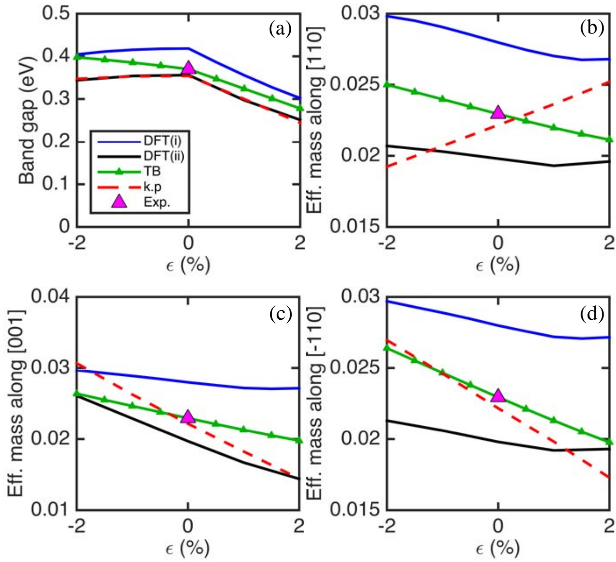

Fig. 4 Same as Fig. 3, but for InAs.

The generally observed trend is that compressive strain increases the effective masses along all directions, whereas tensile strain decreases them. One exception is found for GaAs along [-110] where the opposite trend is observed.

B. Strained $In_{0.53}Ga_{0.47}As$ Ultra-Thin Body Channels

Since $In_{0.53}Ga_{0.47}As$ is regarded as the most attractive III-V channel n-type material for CMOS applications [19], the UTBs in this section are made out of this material.

Following the discussion in Section IV.A, TB was preferred to **k.p** for accuracy reasons. DFT(i) was preferred to DFT(ii) mainly for computational reasons. Only the uniaxial strain case will be discussed from now on since the results obtained for biaxial strain are very similar.

1) Band gap and effective masses

As shown in Fig. 5, DFT(i) predicts only minor differences in the effect of strain between bulk and UTB structures. Compressive strain does not modify E_G for bulk, but it slightly decreases it in confined structures. Strain has no impact on the bulk effective mass along [-110], which can be explained by looking at the opposite strain behavior between GaAs (Fig. 3(d)) and InAs (Fig. 4(d)). With confinement, however, strain starts to influence this effective mass similarly to what is observed in bulk GaAs. The stronger the confinement, the higher the slope. This trend change when going from bulk to UTB (see (*) on Fig. 5 (c)) has been confirmed by DFT(ii) (not shown here), though it was less pronounced there. While this observation is certainly worth further investigations, the small changes in magnitude cannot be expected to play a significant role in realistic devices. With TB (Fig. 6), no significant difference between bulk and UTBs is observed.

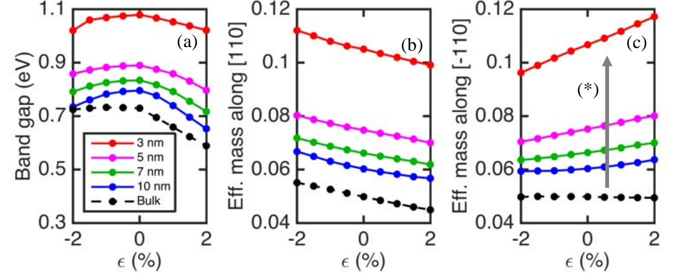

Fig. 5 $In_{0.53}Ga_{0.47}As$ slabs under uniaxial strain simulated with DFT(i). (a) Band gap at Γ. (b) Electron effective mass (units of m_0) along the [110] crystal axis. (c) Same as (b), but along [-110].

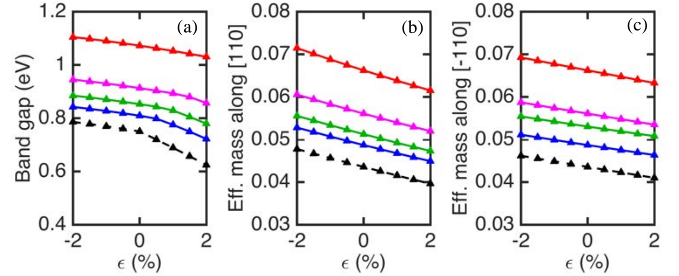

Fig. 6 Same as Fig. 5 , but simulated with TB (identical legend).

2) Impact of strain on the drive current

Though all models predict noticeable changes in m^* between unstrained and strained cases, it is difficult to predict improvements on drive currents without actually doing device simulations. A simple approach based on the ToB model [3] is therefore used to compute the gate capacitance C_G and injection velocity v_{inj} of the $In_{0.53}Ga_{0.47}As$ UTBs, providing a straightforward way to predict performance improvements in ON current, the latter being proportional to the product $C_G v_{inj}$.

In this model, the MOSFET is reduced to a single point described by its potential energy (U_{SC}) and charge density (n_d). At equilibrium, these two quantities are related to each other by the following system of equations:

$$\begin{cases} U_{sc} = U_{sc0} - \alpha_G V_{gs} - \dfrac{q}{C_{ox}} n_d \\ n_d = \dfrac{1}{4\pi^2} \displaystyle\iint_{BZ} \dfrac{1}{1+e^{\frac{U_{sc}+E(k_x,k_z)-E_f}{k_B T}}} dk_x dk_z \end{cases} \quad (1)$$

The gate control factor α_G, oxide capacitance C_{ox}, Fermi level E_f, and the position of the ToB in the unbiased case U_{sc0} are adjusted to obtain a sub-threshold slope of 70 mV/dec at T = 300 K for a given body thickness t_B. The values for t_B = 5 nm (only value presented here) are α_G = 0.85, C_{ox} = 10.1

μF/cm^2, E_f = 0 eV and U_{sc0} = 0.3 eV. The integral in the second equation of (1) is performed in the entire 2D first Brillouin zone (BZ). Spin degeneracy is already included in the band structure $E(k_x,k_z)$.

At a given gate-source bias V_{gs} and 2D band structure $E(k_x,k_z)$, (1) can be solved self-consistently. The gate capacitance is obtained by taking the derivative of n_d with respect to V_{gs} multiplied by the elementary charge. This procedure automatically accounts for the quantum capacitance effect. The injection velocity v_{inj} of electrons is calculated as the average group velocity including all conduction sub-bands:

$$v_{inj}=\frac{1}{\hbar}\frac{1}{4\pi^2 n_d}\iint_{BZ}\frac{\left|\frac{dE(k_x,k_z)}{dk_x}\right|}{1+e^{\frac{U_{sc}+E(k_x,k_z)-E_f}{k_B T}}}dk_x dk_z \qquad (2)$$

Where $\hbar$ is the reduced Plank constant.

As seen in Fig. 7, both tensile and compressive strain affect C_g, implying that the studied devices operate in the quantum capacitance limit (low equivalent oxide thickness of 0.68 nm). Compressive strain leads to improvements in C_g, which can be attributed to a higher transverse effective mass along [-110]. v_{inj} decreases as a result of the heavier electrons along the transport direction [110]. The opposite behavior occurs in the case of tensile strain, where the already marginal improvement of v_{inj} is almost cancelled out by a deterioration of C_g. Taking the product $C_g\, v_{inj}$ for an estimate of the drive current reveals that less than 2% ON-state performance improvement can be expected from these realistic compressive or tensile strain situations. While the opposite trends between $m^*_{[110]}$ and $m^*_{[-110]}$ predicted by DFT(i) for the thinnest films (recall Fig. 5 (b) and (c)) might possibly lead to a somewhat larger increase in drive current, the absolute variations of the masses are not sufficient (they are very similar to TB) to have any tangible effect, especially knowing that this phenomenon is likely overestimated (comparison with DFT(ii), Sec. IV.B).

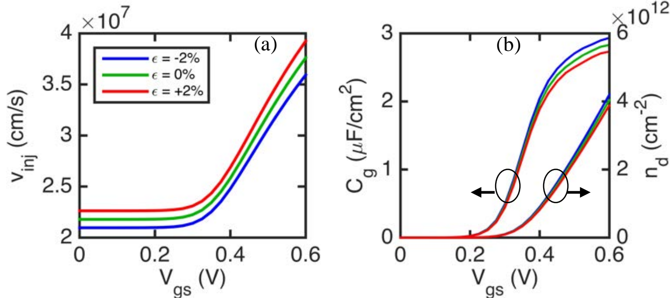

Fig. 7 Electron injection velocity v_{inj} (a), gate capacitance C_g and ToB charge n_d (b) with respect to gate-source bias V_{gs} in the 2% uniaxially compressed (blue), unstrained (green) and 2% extended case (red) in a 5 nm thick $In_{0.53}Ga_{0.47}As$ slab.

V. Conclusions

The detailed analysis of bulk and UTB band structure parameters of GaAs, InAs and $In_{0.53}Ga_{0.47}As$ has provided some important insights into their behavior under realistic biaxial and uniaxial strain configurations. Results from two *ab-initio* methods were used to assess the accuracy of empirical TB and **k·p** for future self-consistent simulations of strained MOSFETs. While all models agree quite well for biaxial strain, some irreconcilable differences between **k·p** and the other models were observed for the effective masses along [110] in the uniaxial case. Due to the limited impact of strain on critical transport parameters such as inversion charge, total gate capacitance and injection velocity, none of the studied strain configurations were found to significantly improve the intrinsic performance of these idealized devices.

Acknowledgment

The research leading to these results has received funding from the European Commission's Seventh Framework Programme (FP7/2007-2013) under Grant Agreement III-V-MOS Project No. 619326 via the IUNET Consortium.

References

[1] M. L. Lee, E. A. Fitzgerald, M. T. Bulsara, M. T. Currie and A. Lochtefeld, "Strained Si, SiGe, and Ge channels for high mobility metal oxide field effect transistors" *J. Appl. Phys*. Vol.97, 2005.

[2] J. A. del Alamo, "Nanometre-Scale electronics with III-V compound semiconductors," Nature, vol. 479, pp. 317-323, 17 Nov. 2011.

[3] A. Rahman, J. Guo, S. Datta, and M. S. Lundstrom, "Theory of ballistic nanotransistors", *IEEE Trans. Elec. Dev.* 50, 1853 (2003).

[4] "ATK-2015." [Online]. Available: www.quantumwise.com.

[5] F. Tran and P. Blaha, "Accurate band gaps of semiconductors and insulators with a semilocal exchange-correlation potential," *Phys. Rev. Lett.* 102, 226401 (2009).

[6] "VASP." [Online]. Available: http://cms.mpi.univie.ac.at/vasp/vasp.pdf.

[7] J. Heyd, G. Scuseria and M. Ernzerhof, "Hybrid functionals based on a screened Coulomb potential", *J. Chem. Phys.* 124, 219906 (2006).

[8] G. Kresse and J. Furthmuller, "Efficient iterative schemes for ab initio total-energy calculations using a plane-wave basis set", *Phys. Rev. B* 54, 11169 (1996).

[9] P. A. Khomyakov, M. Luisier, A. Schenk, "Compositional bowing of band energies and their deformation potentials in strained InGaAs ternary alloys: A first-principles study", APL 107, 062104 (2015).

[10] M. Luisier, A. Schenk, W. Fichtner, G. Klimeck, "Atomistic simulation of nanowires in the sp3d5s* tight-binding formalism: from boundary conditions to strain calculations". *Phys. Rev. B* 74, 205323 (2006).

[11] T. B. Boykin, G. Klimeck, R. Chris Bowen, and F. Oyafusso, "Diagonal parameter shifts due to nearest-neighbor displacements in empirical tight-binding theory", *Phys. Rev. B* 66, 125207 (2002).

[12] M. Luisier and G. Klimeck, "Investigation of $In_xGa_{1-x}As$ Ultra-Thin-Body Tunneling FETs using a Full-Band and Atomistic Approach", SISPAD 2009, San Diego CA, USA (2009).

[13] T. Bahder, "Eight-band k.p model of strained zinc-blende crystals," *Phys. Rev. B* 41, 11992 (1990).

[14] T. Bahder, "Erratum: Eight-band k.p model of strained zinc-blende crystals [Phys. Rev. B41, 11992 (1990)]," *Phys. Rev. B*46, 9913 (1992).

[15] S. Kim, M. Yokoyama, N. Taoka, R. Nakane, T. Yasuda, O. Ichikawa, "Strained $In_{0.53}Ga_{0.47}As$ metal-oxide-semiconductor field-effect transistors with epitaxial based biaxial strain". APL 100, 193510 (2012).

[16] "NSM Archive - Physical properties of semiconductors." [Online]. Available: http://www.ioffe.rssi.ru/SVA/NSM/Semicond/index.html.

[17] I. Vurgaftman, J. R. Meyer, L. R. Ram-Mohan, "Band parameters for III-V compound semiconductors and their alloys", *J. Appl. Phys.* 89, 5815 (2001).

[18] Y. Sun, S. E. Thompson, T. Nishida, "Strain effect in semiconductors: theory and device applications" Springer, ISBN 978-1-4419-0551-2, pp. 9-18 (2010).

[19] J. A. del Alamo, D. Antoniadis, A. Guo, D.-H. Kim, T.-W. Kim J. Lin, "InGaAs MOSFETs for CMOS: Recent advances in process technology", Proc. IEDM, 2013, pp. 24–27.